Continuously tunable slow-light device consisting of heater-controlled silicon microring array

Fumihiro Shinobu,[1,2,*] Norihiro Ishikura,[1,2] Yoshiki Arita,[1,2] Takemasa Tamanuki,[1] and Toshihiko Baba[1,2]

[1]*Department of Electrical and Computer Engineering, Yokohama National University, 79-5 Tokiwadai, Hodogaya-ku, Yokohama, 240-8501, Japan*
[2]*Core Research for Evolutional Science and Technology, Japan Science and Technology Agency, 5 Sanbancho, Chiyoda-ku, Tokyo, 102-0075, Japan*
*baba@ynu.ac.jp

Abstract: We experimentally demonstrate a tunable slow-light device consisting of all-pass Si microrings. A compact device of 0.014 mm^2 footprint is fabricated by using CMOS-compatible process, and its center wavelength, bandwidth and delay are continuously tuned by integrated heaters. The tuning range is 300 ps at fixed wavelengths with a 1 nm bandwidth. Eye opening of 40 Gbps non-return-to-zero signals is observed at up to a 150 ps delay and a 4 bit buffering capacity is confirmed, which corresponds to a spatial buffering density of 0.29 kbit/mm^2.

OCIS codes: (230.3120) Integrated optics device; (230.5750) Resonators.

References and links

1. R. S. Tucker, P.-C. Ku, and C. Chang-Hasnain, "Slow-light optical buffers - capabilities and fundamental limitations," J. Lightwave Technol. **23**(12), 4046–4066 (2005).
2. T. Baba, "Slow light in photonic crystals," Nat. Photonics **2**(8), 465–473 (2008).
3. T. Baba, T. Kawaaski, H. Sasaki, J. Adachi, and D. Mori, "Large delay-bandwidth product and tuning of slow light pulse in photonic crystal coupled waveguide," Opt. Express **16**(12), 9245–9253 (2008).
4. J. Adachi, N. Ishikura, H. Sasaki, and T. Baba, "Wide range tuning of slow light pulse in SOI photonic crystal coupled waveguide via folded chirping," IEEE J. Sel. Top. Quantum Electron. **16**(1), 192–199 (2010).
5. J. Yang, N. K. Fontaine, Z. Pan, A. O. Karalar, S. S. Djordjevic, C. Yang, W. Chen, S. Chu, B. E. Little, and S. J. B. Yoo, "Continuously tunable, wavelength-selective buffering in optical packet switching network," IEEE Photon. Technol. Lett. **20**(12), 1030–1032 (2008).
6. W. M. J. Green, H. F. Hamann, L. Sekaric, M. J. Rooks, and Y. A. Vlasov, "Ultra-compact reconfigurable silicon optical devices using micron-scale localized thermal heating," Tech. Dig. Opt. Fiber Commun. Conf., OtuM3 (2007).
7. J. Cardenas, M. A. Foster, N. Sherwood-Droz, C. B. Poitras, H. L. R. Lira, B. Zhang, A. L. Gaeta, J. B. Khurgin, P. Morton, and M. Lipson, "Wide-band continuously tunable optical delay line using silicon microring resonators," Opt. Express **18**(25), 26525–26534 (2010).
8. A. Melloni, F. Morichetti, C. Ferrari, and M. Martinelli, "Continuously tunable 1 byte delay in coupled-resonator optical waveguides," Opt. Lett. **33**(20), 2389–2391 (2008).
9. A. Melloni, A. Canciamilla, C. Ferrari, F. Morichetti, L. O'Faolain, T. F. Krauss, R. De La Rue, A. Samarelli, and M. Sorel, "Tunable delay lines in silicon photonics: coupled resonators and photonic crystals, a comparison," IEEE Photon. J. **2**(2), 181–194 (2010).
10. Q. Li, F. Liu, Z. Zhang, M. Qiu, and Y. Su, "System performances of on-chip silicon microring delay line for RZ, CSRZ, RZ-DB and RZ-AMI signals," J. Lightwave Technol. **26**(23), 3744–3751 (2008).
11. F. Xia, L. Sekaric, and Y. Vlasov, "Ultracompact optical buffers on a silicon chip," Nat. Photonics **1**(1), 65–71 (2007).
12. K. Okamoto, *Fundamentals of Optical Waveguides*, 2nd ed. (Academic Press, 2000).
13. H. P. Uranus and H. J. W. M. Hoekstra, "Modeling of loss-induced superluminal and negative group velocity in two-port ring-resonator circuits," J. Lightwave Technol. **25**(9), 2376–2384 (2007).
14. T. Tsuchizawa, K. Yamada, H. Fukuda, T. Watanabe, S. Uchiyama, and S. Itabashi, "Low-loss Si wire waveguides and their application to thermooptic switches," Jpn. J. Appl. Phys. **45**(No. 8B), 6658–6662 (2006).
15. J. Cardenas, C. B. Poitras, J. T. Robinson, K. Preston, L. Chen, and M. Lipson, "Low loss etchless silicon photonic waveguides," Opt. Express **17**(6), 4752–4757 (2009).

1. Introduction

Optically tunable delay lines will be applicable for optical buffering, retiming and multi/demultiplexing of pulses, fast pump-probe and correlation measurements, and so on, if they realize wide-range and high-speed tuning of the delay at desired wavelengths while maintaining sufficiently low dispersion [1]. A long delay of over 100 ns is necessary for optical buffering in packet switching, while a 100 ps order delay is already usable in other applications. Aiming for such a delay on a chip, photonic crystal slow light devices have been studied, which greatly reduce the group velocity of light and controls the delay on demand [2]. Here, the localized laser heating deconcentrates the slow light condition spectrally so that the slow light bandwidth is expanded and the delay is reduced accordingly [3]. For example, 250-µm long photonic crystal coupled waveguides on silicon-on-insulator (SOI) substrate achieved a tuning range of up to 100 ps and a tunable buffering capacity of 22 bits for pulses of several picoseconds [4]. A common issue in photonic crystal devices is that they usually employ an airbridge slab structure for the strong optical confinement. It is not straightforward to fabricate the airbridge slab simultaneously with fiber couplers, heaters, PIN junctions, and other waveguide components in Si photonics, and hence this limits the functions added to the delay line. An alternative approach is to use microring resonators in the configurations of all pass filters [5–7] or the mixture of all pass filters and coupled-resonator optical waveguides (CROWs) [8,9]. They also control the delay by locally heating some of multiple rings. A tuning range of up to a few nanoseconds and a tunable buffering capacity of up to 8 bits have been reported for devices in different material systems.
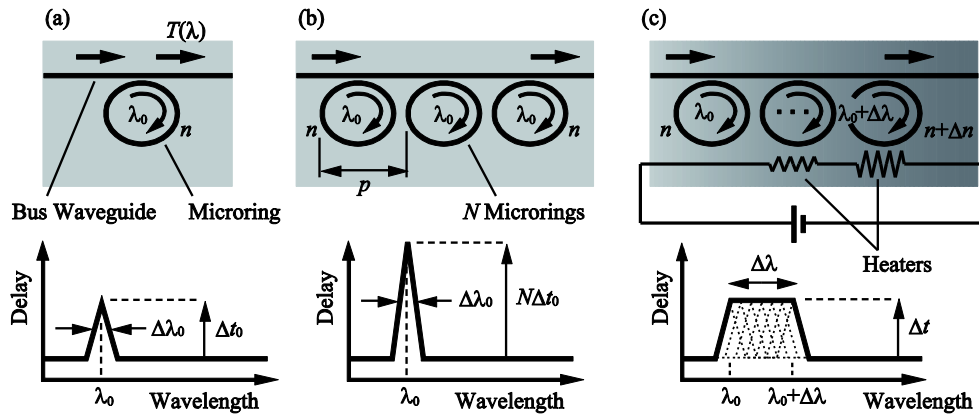

Fig. 1. Schematics of all-pass-type microring array (upper figure) and delay spectrum (lower figure). (a) Single ring model. (b) Multi-ring model with uniform index profile and the same resonant wavelength. (c) Multi-ring model with sloped index profile and detuned resonant wavelengths forming an envelope spectrum.

In this study, we focus on Si microring all pass filters, as schematically illustrated in Fig. 1, because of the following three reasons: (1) high-quality fabrication of Si microrings is available using CMOS-compatible process; (2) the spatial buffering density of Si microrings is higher than those of lower-index-contrast systems, as discussed later; and (3) even with some disordering and imperfection, all pass filters exhibit the smoother spectral characteristics than in CROWs (CROWs usually exhibit a noisy spectrum caused by the small fluctuation in the coupling strength between rings particularly with a high-index contrast). For such a device, fixed delays have been studied for single ring [10] and multiple rings [11]. Tunable delay has also been reported [6,7]. In particular, Ref. [7]. maintains a low-dispersion condition by the balanced detuning of eight rings and demonstrates a tunable capacity of < 2 bits for 10 Gbps signals. Our approach is similar but simpler than this. We integrate many rings, each of which has the same group delay spectrum. Even though small disordering occurs in each ring, the statistical distribution of the spectral detuning is expected to form a smooth envelope spectrum with a maximum delay. The delay is reduced from this value by intentionally

detuning some rings further so that the envelope delay spectrum is expanded in the same manner as in the photonic crystal devices. For the intentional detuning, we also use localized heating. Here, we do not prepare a heater for every ring [6,7] but a smaller number of heaters to form a slope of the detuning. This is effective for simplifying the heater control and making the envelope spectrum smoother.

In this paper, we first summarize the theoretical background indicating the advantage of Si microrings, compared with other material systems. After describing the fabrication, we present the observation of fixed and tunable delays as well as the evaluation of the data transmission quality. We discuss the agreement with the theory, and advantages and issues of this approach.

2. Theory

As shown in Fig. 1, microrings are directionally coupled to the bus waveguide. For such simple configuration, the transmission and slow light characteristics can be derived analytically. We first consider a single ring (Fig. 1(a)), for which the transmission spectrum $T(\lambda)$ is expressed as [12]

$$T(\lambda) = 1 - \frac{(1-A)(1-T_0)}{\left(1-\sqrt{AT_0}\right)^2 + 4\sqrt{AT_0}\sin^2\left(\pi n_{eq}\ell/\lambda\right)} \tag{1}$$

where T_0 is the single pass transmittance at the directional coupling, A is the single round trip loss in the ring defined as $A \equiv e^{-\alpha\ell}$ ($A \sim 1$ in many cases), α is the average loss coefficient in the ring including waveguide loss, bend loss, and the scattering loss at the directional coupling, ℓ is the orbital length of the ring, and n_{eq} is the modal equivalent index of the waveguide. Then the full width at half maximum of the resonance, $\Delta\lambda_0$, is derived as

$$\Delta\lambda_0 = C_1\lambda_0^2/\pi n_g\ell \quad \text{for} \quad C_1 \equiv T_0^{-1/4} - T_0^{1/4} \tag{2}$$

where n_g is the group index of the waveguide. At the resonant wavelength λ_0, the loss L_0 and delay Δt_0 occur due to round trips in the ring. Expressions for them in Refs. [12,13]. can be modified as

$$L_0 = 4.34(C_2/C_1)\alpha\ell \; [\text{dB}], \quad \Delta t_0 = (C_2/C_1)n_g\ell/c \quad \text{for} \quad C_2 \equiv T_0^{-1/4} + T_0^{1/4} \tag{3}$$

We can see from Eqs. (2) and (3) that $\Delta\lambda_0$ decreases while L_0 and Δt_0 increase when T_0 approaches unity. For any slow light device, the delay-bandwidth product $DBP \equiv \Delta t\Delta f$ constrains the buffering capacity [1,2]. Let us consider the buffering of Gaussian pulses, each having an ideal time-bandwidth product of 0.441, and also consider a Lorentzian response of the ring approximated from Eq. (1) around λ_0. The time-bandwidth product of the pulses increases to 0.693 after they pass through the ring having the same bandwidth as the pulse's. Then, the buffering capacity M [bit] is give by $\eta DBP/0.693 = 1.44\eta DBP$, where η is the spectral efficiency defined as the ratio of the pulse bandwidth to the ring bandwidth. From these equations,

$$DBP = 0.318C_2, \quad M = 0.459\eta C_2 \tag{4}$$

Note that DBP and M are independent of the ring size because a larger ring gives a longer delay and a narrowed bandwidth. From Eqs. (3) and (4), the buffering loss is given by

$$L_0/M = 9.46\alpha\ell/\eta C_1 \; [\text{dB/bit}] \tag{5}$$

The pitch p in Fig. 1(b) can be regarded as the longitudinal length of the device. Then, p and the device footprint S_0 of the single ring model are approximated as

$$p = (\ell / \pi)(1+\delta), \quad S_0 = (\ell / \pi)^2 (1+\delta) \tag{6}$$

where δ is a correction factor expressing a modified shape of the ring from the circular one (e.g. racetrack) and the space between the rings. The effective group index n_{geff} of the device is give by

$$n_{\text{geff}} = c\Delta t_0 / p = \pi n_g (C_2 / C_1)/(1+\delta) \tag{7}$$

The normalized delay-bandwidth product $n_{\text{geff}}(\Delta\lambda_0/\lambda_0)$ [2] is often used as the figure of merit *FOM* of slow light, and *FOM* leads the spatial buffering density such that

$$FOM = \lambda C_2 / \ell(1+\delta), \quad M / S = 4.53\eta FOM / \lambda\ell \tag{8}$$

Equations (6) and (8) indicate that a smaller ℓ directly contributes to reducing the footprint, as well as enhancing *FOM* and the buffering density. (This is not the case for photonic crystal devices; *FOM* is independent of the device length while *DBP* and *M* increase with the length.) For the microring, ℓ can be reduced by employing a high-index-contrast waveguide. This is the reason that we employ Si wire waveguides in this study rather than other low-index-contrast waveguides. Equations (3) and (5) also imply that the loss could be reduced by a small ℓ. However, it is not straightforward because high-index-contrast waveguides usually have a larger α due to the stronger light scattering from the disordering in fabricated devices.

So far, the single ring has been discussed. When the bus waveguide is coupled with isolated *N* rings having the same λ_0 (Fig. 1(b)), $T(\lambda)$ is given by multiplying Eq. (1) *N* times. Here, the second term in Eq. (1) is much smaller than unity in many cases. Therefore, $T(\lambda)$ is approximated as

$$T(\lambda) \approx 1 - \frac{N(1-A)(1-T_0)}{\left(1-\sqrt{AT_0}\right)^2 + 4\sqrt{AT_0}\,\sin^2\left(\pi n_{\text{eq}}\ell/\lambda\right)} \tag{9}$$

Under this condition, the total loss *L*, delay Δt, *DBP* and footprint *S* simply become *N* times larger, maintaining almost the same $\Delta\lambda_0$. On the other hand, when rings have different λ_0 due to the localized index change (Fig. 1(c)), the second term of Eq. (1) is replaced by the sum of all rings' when the same approximation as for Eq. (9) is used, i.e.

$$T(\lambda) \approx 1 - \sum_{i=1}^{N} \frac{(1-A)(1-T_0)}{\left(1-\sqrt{AT_0}\right)^2 + 4\sqrt{AT_0}\,\sin^2\left(\pi n_{\text{eq}}^{(i)}\ell/\lambda\right)} \tag{10}$$

In this case, $\Delta\lambda$ of the envelope spectrum becomes larger than $\Delta\lambda_0$, and *L* and Δt are reduced. Their minimum values will be the same as those for the single ring model when the spectra are completely split.

3. Fabrication

In the fabrication, CMOS-compatible process (8 inch SOI wafer, KrF stepper exposure) was used. Silica-clad Si wires of 0.40 μm width and 0.22 μm height are used for both bus waveguide and rings. For this waveguide, n_g is calculated by using finite element method to be 4.2 at $\lambda = 1.53$ μm. The bus waveguide is terminated at input and output ends by inverse-taper-type fiber coupler, where the tip width of the Si inverse taper is 0.18 μm and the end waveguides are silica rectangular channels of $(4 \text{ μm})^2$ cross-section. The coupling loss from lensed single mode fiber of 3 μm spot diameter to the bus waveguide is ~3.5 dB on each side (this loss can be reduced to 0.4 dB if the tip width is narrowed to 80 nm [14]). The propagation loss is measured to be $3 - 5$ dB/cm for the transverse-electric polarization at $\lambda =$

1.53 − 1.56 μm. The typical insertion loss from fiber to fiber through 2-mm-long Si wire is ~10 dB.

Figure 2 shows the optical micrograph of the fabricated device. Racetrack rings of 6 μm bend radius are coupled with the bus waveguide with a coupling length of 4.5 μm (ℓ = 46.7 μm). The free spectral range of the resonance is calculated from n_g and ℓ to be 11.9 nm at λ = 1.53 μm. When the gap between the waveguide and ring, g, is 0.23 μm, T_0 is calculated to be 0.65 by using three-dimensional finite-difference time-domain simulation. The scattering loss at the coupling is also calculated to be 0.4%. Considering this value and an average waveguide loss of 4 dB/cm, α is estimated to be 1.84 cm^{-1}, which ensures the above assumptions that A ~1 and the second term in Eq. (1) is much smaller than unity. Substituting these values into Eqs. (2)–(4) gives $\Delta\lambda_0$ = 0.84 nm, L = 0.35N [dB], Δt = 6.1N [ps] and DBP = 0.64N. Provided that the total insertion loss including the fiber coupling must be less than 30 dB so that the loss can be recovered by standard optical amplifier, N is set at 50, for which we calculate L = 17.4 dB, Δt = 305 ps and DBP = 32.

The space between adjacent rings is limited to 5 μm. Therefore, δ for this space and the racetrack shape is 0.3. The total device length $p(1 + \delta)N$ is 1060 μm, and the total footprint $S = S_0N$ only counting rings and the bus waveguide is as small as 0.014 mm^2. From these values, Eqs. (4), (5), (7), (8) predict M = 46η [bits], L_0/M = 0.38/η [dB/bit], n_{geff} = 95, FOM = 0.051, and M/S = 3.2η [kbit/mm^2].
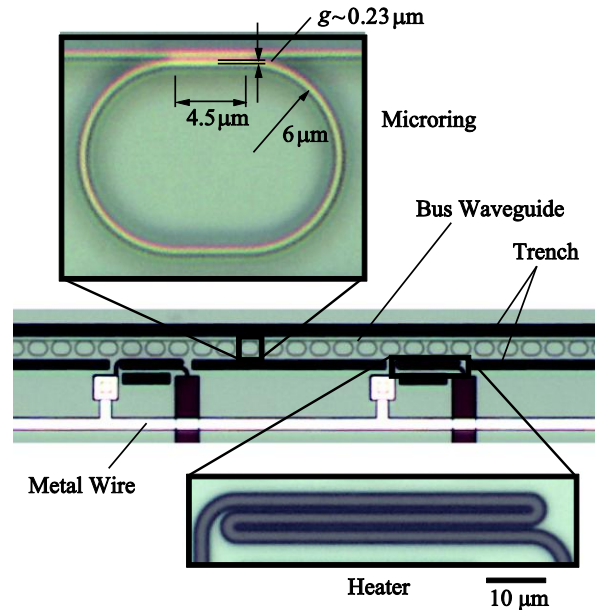

Fig. 2. Optical microscope images of fabricated device.

4. Measurement

Transmission and group delay spectra were measured by using dispersion analyzer Alnair FDA-2100 based on the modulation phase-shift method, where the delay in the Si wire without rings is used as a reference. Figure 3(a) shows the results for three different g. The spectral dip and delay peak are very simple and smooth, which may be difficult to obtain in CROW. Such a dip and peak were observed periodically with a free spectral range of 11.9 nm at λ ~1.53 μm. It completely agrees with the aforementioned calculated value, which assures that other calculated values are also correct. The delay and loss at the resonance increase with increasing g. At g = 0.23 μm, the experimentally measured values are $\Delta\lambda$ = 1.0 nm, L = 18 dB,

$\Delta t = 300$ ps, $DBP = 36$, $n_{geff} = 85$ and $FOM = 0.056$, all of which are in good agreement with theoretical values. This FOM is $4 - 5$ fold smaller than typical values of $0.2 - 0.3$ for photonic crystal devices. It is a reasonable result because the phase shift at the resonance of rings is smaller than that of photonic crystals under the slow light condition.

Next, we discuss the delay tuning, which is the major difference from Ref. [11]. reporting a large-scale integration of similar all-pass Si microrings. In the fabricated device, five TiN heaters were placed beside the rings with 200 µm pitch, as shown in Fig. 2. In addition, eight heaters were placed outside of the area of Fig. 2. Around the inner heaters and between inner and outer heaters, some trenches are perforated through the silica clad to the Si substrate to improve the heating efficiency and suppress the thermal crosstalk. Inner heaters, each of which is controlled independently, are used to form a temperature slope and tune the delay and bandwidth. As the dispersion analyzer can acquire one delay spectrum within a few seconds, we can form a desired envelope spectrum by repeating the measurement while controlling the inner heaters. However, overall the spectrum redshifts due to some thermal crosstalk when only using the inner heaters. Therefore, the outer heaters are also used to heat the device uniformly when the inner heaters are not used heavily, so that the spectral peak is always redshifted and located at the same wavelength. Figure 3(b) shows the change of the delay spectrum with heating. Here, the target wavelength is set at 3.5 nm longer than that without heating (near 1532 nm), which maximizes the tuning range, avoiding severe thermal crosstalk. Values in this figure denote the total heating power. Many of them have similar values, but the power balance between heaters is changed variously. The power values might be higher than normal for microrings, because the heating from the side is not so efficient. In this experiment, we could not form top heaters above the rings due to the restriction of multiple-project wafer process. If top heaters can be used, the power will be reduced significantly. At the target wavelength, the delay Δt is controlled in the range of $4 - 300$ ps. At $\Delta t \geq 150$ ps, Δt and the bandwidth are changed continuously while maintaining the peak wavelength. At $\Delta t = 150$ ps, a flat top spectrum of 1.3 nm width is obtained. At $\Delta t < 150$ ps, the heating power to the inner heaters increased and the thermal crosstalk became severer. Since the temperature slope was not sufficient under this condition, it was difficult to expand the bandwidth further at the same wavelength. Therefore, we simply blueshifted the peak wavelength by reducing the total power so that Δt decreases to 4 ps at its minimum.
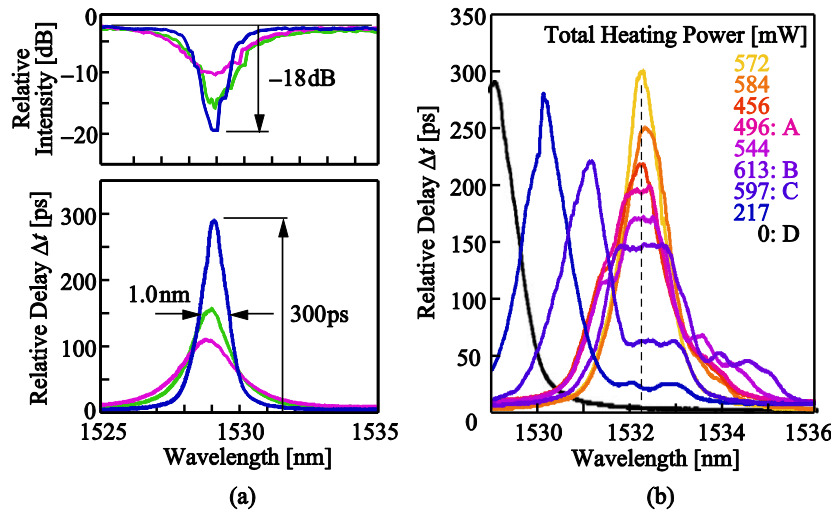

Fig. 3. Transmission and delay spectra. (a) Dependence on gap g without heating. Red, green and blue correspond to $g = 0.19$, 0.21 and 0.23 µm, respectively. (b) Change of delay spectrum with heating for $g = 0.23$ µm.

To confirm the transmission quality of optical signals with delays, eye diagrams and serial bit patterns were observed for 40 Gbps non-return zero (NRZ) 2^7-1 pseudo-random bit sequence (PRBS), as shown in Fig. 4. At $\Delta t \leq 150$ ps, the eye opening is observed with the clear bit pattern, for which we can confirm the tunable buffering capacity of $M = 4$ bits, the buffering density $M/S = 0.29$ kbit/mm^2, and the buffering loss $L/M = 3.5$ dB/bit. At $\Delta t > 150$ ps, the eye closes although the pattern can still be recognized. It might be affected by a dispersion larger than 10 ps/nm. It can be reduced by suppressing the thermal crosstalk and controlling the local temperature minutely. D exhibits a delay of 184 ps = 7.3 bit, which agrees with the result in Fig. 3(b) and is also consistent with the theoretical prediction that M ~9 bit and M/S ~0.64 kbit/mm^2 at the maximum delay when we assume η ~0.2 approximated for the PRBS signals against the spectral response without heating in Fig. 3(a).
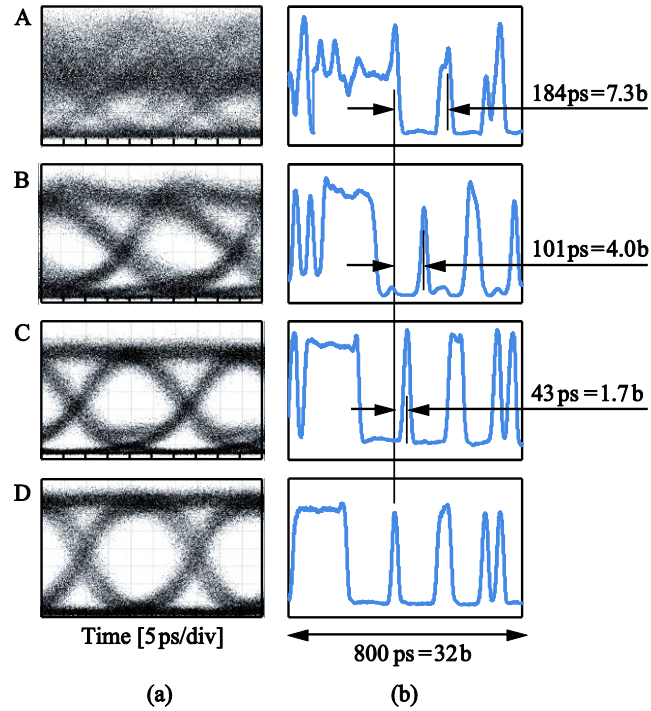

Fig. 4. Eye diagram (a) and bit pattern (b) of 40 Gbps NRZ 2^7-1 PRBS signal output from the device. A-D correspond to those in Fig. 3.

5. Discussion

In this study, we employed all-pass microrings for tunable delay, rather than photonic crystals and CROWs because of the ease of fabrication and the spectral robustness, respectively. As understood from Eqs. (4) and (9), the buffering capacity of each ring is constant for any design and material system, and the spatial buffering density is simply enhanced by downsizing each ring. For this purpose, the high-index-contrast Si wire waveguide can be an ideal platform. Since our device employed a very compact arrangement of rings and simpler bus waveguide, the footprint is as small as 0.014 mm^2, which is much smaller than 0.09 mm^2 for a similar device [11] and even smaller than 0.025 mm^2 for a Si microring CROW [9]. Therefore, even comparing our tunable delay with the fixed delay in Ref. [11], our buffering density is 2.6 times larger. Of course, it is $2 - 3$ orders higher than those in low-index-contrast systems [5,8]. The delay may be enhanced up to 1 ns with 200 microrings, for which the device footprint is still reasonably small (< 0.06 mm^2). In a larger array, the fine control of local temperatures will be easier, so the dispersion will be more suppressed. The main issue is

the reduction of loss. The buffering loss in this study is $3 - 5$ times higher than those of low-index-contrast systems, and the total loss for a 1 ns delay cannot be recovered by optical amplifier. At the very least, the buffering loss will be reduced to a comparable level and the total loss will be acceptable by suppressing the scattering loss at the directional coupling by optimizing the design and by using the state-of-the-art Si photonics technology, which has already achieved a waveguide loss of 2 dB/cm [14]. Further enhancement of the delay and capacity simply depends on a lower waveguide loss without losing the compactness of the ring. Other novel process is worth investigating for this purpose [15].

Acknowledgments